Original Article

Manipulating Histone Acetylation Leads to Adverse Effects in Hemangiosarcoma Cells

Tamami Suzuki [a], Keisuke Aoshima [a,] *, Jumpei Yamazaki [b], Atsushi Kobayashi [a], Takashi Kimura [a]

[a] *Laboratory of Comparative Pathology, Department of Clinical Sciences, Faculty of Veterinary Medicine, Hokkaido University, Sapporo, Hokkaido, 060-0818, Japan*
[b] *Translational Research Unit, Veterinary Teaching Hospital, Faculty of Veterinary Medicine, Hokkaido University, Sapporo, Hokkaido, 060-0818, Japan*

* Corresponding author. Tel.: +81 11 7065193.
E-mail address: k-aoshima@vetmed.hokudai.ac.jp (Keisuke Aoshima).

Abstract

Canine hemangiosarcoma (HSA) is a malignant tumour derived from endothelial cells. No effective treatment has yet been developed because of the lack of understanding of its pathogenesis. Histone acetylation, an epigenetic modification, is highly associated with cancer pathogenesis. Manipulating histone acetylation by histone deacetylase inhibitors (HDACi) or bromodomain and extraterminal domain inhibitors (BETi) is one approach to treat various cancers. However, the role of histone acetylation in HSA remains unknown. This study aimed to investigate how histone acetylation functions in HSA pathogenesis using two HDACi, suberanilohydroxamic acid (SAHA) and valproic acid (VPA), and one BETi, JQ1, *in vitro* and *in vivo*. Histone acetylation levels were high in cell lines and heterogeneous in clinical cases. SAHA and JQ1 induced apoptosis in HSA cell lines. SAHA and VPA treatment in HSA cell lines upregulated inflammatory-related genes, thereby attracting macrophages. This implies that SAHA and VPA can induce anti-tumour immunity. JQ1 stimulated autophagy and inhibited the cell cycle. Finally, JQ1 suppressed HSA tumour cell proliferation *in vivo*. These results suggest that HDACi and BETi can be alternative drugs for HSA treatment. Although further research is required, this study provides useful insights for developing new treatments for HSA.

Keywords: BETi; HDACi; hemangiosarcoma; histone acetylation

Introduction

Canine hemangiosarcoma (HSA) is an aggressive malignant tumour derived from endothelial cells. Surgery and chemotherapy are conventional therapies for HSA, but a review article summarised that the efficacy of these treatments was limited (Clifford et al., 2000). No other treatments are available because little is known about the detailed molecular pathogenesis of HSA. Thus, more basic research on HSA is warranted.

Epigenetics such as DNA methylation and histone modifications regulates transcription without altering DNA sequences, and these mechanisms are involved in various biological processes such as embryonic development, metabolism, and diseases, including cancer (Kaelin and McKnight, 2013; Virani et al., 2012; Xu et al., 2021). Acetylated histone can promote transcription by binding to bromodomain and extraterminal (BET) proteins and loosening the chromatin structure by neutralizing the electric charges between histone and DNA (Josling et al., 2012; Clayton et al., 2006).

In recent years, a growing number of reports have highlighted that histone acetylation is involved in cancer pathogenesis (Calcagno et al., 2019; Liu et al., 2018). Histone deacetylase inhibitors (HDACi) and BET inhibitors (BETi) have been used to investigate the function of histone acetylation and their treatment efficacy. HDACi inhibits histone deacetylase function, thereby increasing histone acetylation levels (West and Johnstone, 2014). BETi binds to the functional domain of BET proteins through which BET proteins cannot recognise acetylated histones (Bechter and Schöffski, 2020). Suberanilohydroxamic acid (SAHA) and valproic acid (VPA) are HDACis that have been reported to induce apoptosis and cell death *in vitro* and suppress tumour proliferation *in vivo* in various human cancers (Claerhout et al., 2011; Lee et al., 2012; Uehara et al., 2012; Yagi et al., 2010). HDACi can also improve tumour immunity, and combination therapies with immune checkpoint inhibitors or chemotherapeutics enhance their efficacy in human cancers

(Huang et al., 2017; Kim et al., 2020; Xue et al., 2016). BETi has also been broadly investigated as cancer drugs, including JQ1, which can cause apoptosis, cell cycle arrest, and autophagy *in vitro*, and impede tumour growth *in vivo* (Jostes et al., 2017; Li et al., 2019; Wen et al., 2019).

Regarding epigenetics in HSA, KDM2B—a histone demethylase—has recently been found to promote tumour viability by enhancing the DNA damage response (Gulay et al., 2021). However, the role of histone acetylation in HSA remains unknown. In this study, we aimed to investigate the role of histone acetylation and the effects of HDACi and BETi on HSA.

Materials and Methods

Histopathology and immunohistochemistry (IHC)

Tumour samples were obtained from patients presenting to Hokkaido University Veterinary Teaching Hospital with written informed consent (Table S1). Haematoxylin and eosin staining was performed as previously described (Maharani et al., 2018). IHC analysis was performed as previously described (Gulay et al., 2021) with slight modifications described below. Heat-induced antigen retrieval was performed twice in Tris-EDTA buffer (pH 9.0) in a microwave for 5 min. Tissues were stained with anti-acetylated histone H3 antibody (1:250; #39140, Active Motif, CA, USA) overnight at 4°C. Quantification of IHC results using QuPath was performed based on Nucleus DAB OD mean, and the values of acetylated histone H3 in tumour cells were normalised against those in normal endothelial cells on the same slides for further analysis (Bankhead et al., 2017).

Cell culture

Normal canine aortic endothelial cells (CnAOEC: #Cn304-05, Cell Applications, CA,

USA), seven canine HSA cell lines (JuA1, JuB2, JuB4, Re12, Re21, Ud2, and Ud6. (Murai et al., 2012), ISOS-1 obtained from the Cell Resource Center for Biomedical Research Cell Bank (Tohoku University) (Masuzawa et al., 1998), and RAW264 obtained from RIKEN Bioresource Center were cultured with Dulbecco's Modified Eagle Medium High Glucose (DMEM; #044-29765, Fujifilm Wako Pure Chemical Industries, Osaka, Japan) supplemented with 10% foetal bovine serum (FBS; #S1580-500, Biowest, UT, USA) and penicillin–streptomycin solution (#168-23191, Fujifilm Wako) at 37□ with 5% CO_2.

Drug preparation

SAHA (#10009929, Cayman Chemical, MI, USA) was initially dissolved in dimethyl sulfoxide (DMSO) to a stock solution of 150 mg/ml. For *in vivo* studies, the stock solution of SAHA was diluted with 30% polyethylene glycol 400 and 5% Tween 80 in double distilled water. VPA (#227-01071, Fujifilm Wako) was dissolved in PBS. JQ1 (#T117580, Toronto Research Chemicals, Toronto, Canada) was initially dissolved in DMSO to a stock solution of 50 mg/ml. For *in vivo* studies, the stock solution of JQ1 was diluted with 5% Tween 80 in PBS.

Cell viability assay

Two thousand cells were seeded in 96-well cell culture plates and cultured in 100 µL culture medium. The next day, they were treated with DMSO, SAHA, or JQ1. Survival rates and growth inhibition rates were analysed as previously described (Aoshima et al., 2018; Morita et al., 2019)[1].

Apoptosis assay

[1] See: NCI 60 Cell Five-Dose Screen. https://dtp.cancer.gov/discovery_development/nci-60/methodology.htm (Accessed 21 October, 2021).

Apoptosis assay was performed using the FITC Annexin V Apoptosis Detection Kit (#556547, BD Biosciences, NJ, USA) according to the manufacturer's instructions. Briefly, JuB4 and Re12 cells were treated with 10 μM SAHA or JQ1 for 24 h, and detached from dishes using TrypLE Express Enzyme (#12604013; Thermo Fisher Scientific). One million cells were suspended in the binding buffer and divided into stained with annexin V. Cells were analysed with a BD FACSVerse flow cytometer (BD Biosciences), and the results were analysed with FCS Express 4 software (De Novo Software, CA, USA).

RNA-Sequencing

ISOS-1 cells were treated with 1 μM SAHA for 24 h, 1 μM JQ1 for 36 h, or 2 mM VPA for 36 h in triplicate. Total RNA was extracted with a NucleoSpin RNA isolation kit (#740955.50, Macherey-Nagel GmbH & Co. Düren, Germany) according to the manufacturer's instructions. RNA samples were submitted to Kazusa DNA Research Institution (Chiba, Japan) for further analyses. RNA-seq libraries were constructed using a QuantSeq 3'mRNA-Seq Library Prep Kit (LEXOGEN, Vienna, Austria) and sequenced with the NextSeq500 (Illumina, CA, USA) to generate a minimum of two million single-end 75-bp reads. Sequencing reads were mapped to the mm39 mouse reference genome using STAR, and expression levels were estimated using RSEM (Dobin and Gingeras, 2015; Li and Dewey, 2011). Differential expression and gene expression profiles were analysed by edgeR and GSEA v4.1.0 (Robinson et al., 2009; Mootha et al., 2003; Subramanian et al., 2005), respectively.

SA-β-gal staining

SA-β-gal staining was performed using a Senescence β-Galactosidase Staining Kit (#9860, Cell Signaling Technology, MA, USA) according to the manufacturer's instructions.

Briefly, ISOS-1 was treated with DMSO or 10 μM JQ1 for 24 h and fixed with 4% paraformaldehyde (PFA) for 10 min at room temperature (RT). Cells were stained with β-Galactosidase Staining Solution containing 5-bromo-4-chloro-3-indolyl β-D-galactopyranoside (X-Gal: #16495, Cayman Chemical) for 13 h at 37□. Cells were covered with 70% glycerol. Positive cells were counted manually using an inverted microscope (BIOREVO BZ-9000; KEYENCE, Tokyo, Japan).

Cell cycle analysis

ISOS-1, JuB2, JuB4, and Re12 cells were treated with DMSO or JQ1 for 24 h. ISOS-1 was treated with 10 μM JQ1, and other cell lines were treated with 5 μM JQ1. Cell cycle analysis was performed as previously described (Gulay et al., 2021).

Migration assay

JuB4 and Re12 were treated with DMSO, 2 μM SAHA, or 2 mM VPA for 48 h in 6-well plates. Then, the medium was replaced to the one without inhibitors, and the cells were co-cultured with RAW264 seeded on ThinCert Cell Culture Inserts (#657630, Greiner Bio-One) for 24 h. RAW264 cells on the culture surface of the inserts were removed with a cotton swab. Migrated RAW264 cells on the bottom side of the inserts were fixed with 4% PFA for 30 min at RT and then stained with 0.01% crystal violet for 30 min at RT. The number of cells was counted manually in 10 fields at 200× under a light microscope (BH-2; Olympus, Tokyo, Japan).

Protein extraction and western blotting

Protein extraction and western blotting were performed as previously described (Gulay et al., 2021). Antibodies used in this study are listed in Table S2.

RNA extraction and reverse transcription quantitative polymerase chain reaction (RT-qPCR)

Primers and samples were prepared as described previously (Gulay et al., 2021). qPCR was performed using the primers listed in Table S3. Results were normalised according to the geometric mean of reference genes (*RPL32* and *HPRT* for canine genes and *Hprt* and *Tbp* for murine genes), which were selected from potential internal controls by geNorm analysis (Fig. S1) (Vandesompele et al., 2002). Relative expression levels were calculated by setting the DMSO-treated cells as the control.

Animal studies

All mouse experiments were performed under the guidelines of Hokkaido University (protocol number: 20-0083), which follows the ARRIVE guidelines. Five-week-old female Balb/c and KSN/Slc mice (Japan SLC, Inc. Shizuoka, Japan) were used. A day before tumour cell inoculation, KSN/Slc mice were treated with 100 μL 2.5 mg/ml anti-asialo GM1 (014-09801, Fujifilm Wako) to increase the success rate of JuB2 transplantation (Yoshino et al., 2000). Five million cells were inoculated subcutaneously in both flanks of Balb/c and KSN/Slc mice, respectively, which were anesthetised with 0.3 mg/kg medetomidine (Domitor, ZENOAQ, Tokyo, Japan), 4 mg/kg midazolam (Dormicum, Maruishi Pharmaceutical Co., Ltd. Osaka, Japan) and 5 mg/kg butorphanol (Vetorphale, Meiji Seika Pharma Co., Ltd. Tokyo, Japan). After tumour cell inoculation, mice were awoken by intraperitoneal injection of 3 mg/kg atipamezole (Atipame, Kyoritsu Seiyaku Corporation, Tokyo, Japan). Tumour volumes were calculated using the formula: Volume = (Length × Width^2)/2. When the tumour volume reached 100 mm^3, mice were treated with the vehicle control or inhibitors. Mice were intraperitoneally injected with SAHA (150 mg/kg) daily, VPA (200 mg/kg) five times weekly, or JQ1 (50 mg/kg) daily. Animals in all experimental groups were examined at least twice

weekly to check their health status and to measure tumour sizes. Balb/c mice were euthanized with CO_2 when tumours reached 1000 mm^3 in volume. KSN/Slc mice were euthanized with CO_2 11 or 12 days after treatment initiation.

Statistical analysis

Statistical analyses were performed with R (version 4.1.0). Fisher's exact test was used to analyse the ratio of acetylated H3 staining levels. Student's *t*-test or Mann-whiteny test were used to analyse the differences between two groups, whereas Tukey's test was used to analyse differences among multiple groups. The significance of the differences in the survival curves of ISOS-1 tumours was analysed using the log-rank test. Overall JuB2 tumour growth was compared using two-way ANOVA.

Results

Histone acetylation levels in HSA cells are high in vitro and heterogeneous in vivo

We first analysed histone acetylation levels in seven HSA cell lines and in CnAOEC normal canine endothelial cells. We found that global acetylation of H2B, H3, and H4 was significantly enriched in all HSA cell lines compared with CnAOEC (Fig. 1A). Then, we examined global acetylated histone H3 levels in 10 clinical HSA cases. These cases were classified into three types according to their histological pattern: solid, capillary, or cavernous (Kim et al., 2015). Five cases had a single histological pattern, while the other five possessed multiple proliferation patterns (Fig, 1B). We also classified histone H3 acetylation levels into three groups according to the normalized values: negative (< 0.5), weak (0.5–2.0), and strong (> 2.0) (Figs. 1C and 1D). The results showed that the histone H3 acetylation levels of tumour cells were heterogeneous, and the ratio was different depending on their histological pattern even in the same tumour tissue (Figs. 1E and 1F). Furthermore, the ratio of tumour cells

classified as negative was the highest in the solid pattern followed by the capillary pattern, and the lowest in the cavernous pattern (Fig. 1F). These results suggest that histone H3 acetylation levels are heterogeneous in tumour cells and are associated with their histopathological patterns.

SAHA and JQ1 induce apoptosis in HSA cell lines

Next, to examine the roles of histone acetylation in HSA pathogenesis, we modified histone acetylation levels using HDACi (SAHA and VPA) and BETi (JQ1). First, we evaluated whether global histone acetylation levels were altered by these inhibitors. SAHA and VPA treatments increased global histone acetylation levels in both canine and murine HSA cell lines, whereas JQ1 decreased them in canine HSA cell lines but not in ISOS-1 (Fig. 2A). Then, we examined the effects of HDACi and BETi on HSA cell proliferation. SAHA and JQ1 treatment significantly decreased the number of cells, while VPA treatment did not affect their proliferation (Fig. 2B). IC_{50} values of the inhibitors in HSA cell lines were almost or less than one-tenth of those in CnAOEC, which indicated that HSA cell lines were more susceptible to these inhibitors than CnAOEC (Fig. 2C). Then, to investigate whether the cells actively died by SAHA or JQ1, we examined apoptosis markers: cleaved caspase 3 and annexin V. The results demonstrated that SAHA and JQ1 increased cleaved caspase 3 expression levels and annexin V positivity in HSA cell lines except for JQ1-treated ISOS-1 cells (Figs. 2D–F). Finally, we evaluated total protein expression and phosphorylation levels of cell survival proteins AKT and ERK. Although the results were different among the cell lines, either total or phosphorylated AKT or ERK levels were downregulated by SAHA and JQ1 but not by VPA (Fig. S2B). These results suggested that SAHA and JQ1 induced apoptosis in HSA cell lines except for ISOS-1 treated with JQ1, and that VPA did not induce cell death in all HSA cell lines.

SAHA and VPA activate inflammatory responses in HSA cell lines

Next, we further investigated the mechanisms of their effects in HSA cells. GSEA results of ISOS-1 cells indicated that inflammatory-related gene expression was positively correlated in SAHA and VPA treatment (Fig. 3A). Consistent with this, *Il6*, *Cxcl1*, *Ccl2*, *Ccl7*, and *Oas1a* were upregulated more than two-fold following treatment with either SAHA or VPA or both (Fig. 3B). We wanted to extrapolate these findings to canine HSA cell lines, but *CXCL1* and *CCL2* do not exist in the canine genome and *CCL7* expression was not detected. However, *OAS1*, the orthologue of murine *Oas1a*, and other inflammatory-related genes were upregulated more than two-fold in canine HSA cell lines treated with SAHA and/or VPA (Fig. 3C). Inflammatory responses in tumour cells can induce immune cell migration, leading to host immune responses to tumour tissues. Therefore, to corroborate whether SAHA and VPA treatment in HSA cell lines can attract immune cells, a macrophage migration assay was performed using RAW264 cells (Fig. 3D). RAW264 cells migrated when they were co-cultured with SAHA-treated JuB4 or VPA-treated Re12 (Fig. 3E).

These results suggest that SAHA and VPA treatment can induce inflammatory responses in HSA cell lines. This could attract macrophages, although it depends on the combination of HSA cell lines and HDACi.

JQ1 treatment induces autophagy and impedes the cell cycle in HSA cell lines

We also investigated the genome-wide gene expression changes in JQ1-treated ISOS-1 cells. GSEA results showed that autophagy-related gene expression and cell cycle related-gene expression were positively and negatively correlated, respectively (Figs 4A and 4B). These expression changes were validated by RT-qPCR (Fig. 4C). LC3-II, an active autophagy marker, was expressed at significantly higher levels in all JQ1-treated HSA cell lines except

for Re12 compared with DMSO controls (Fig. 4D).

Then, we generated growth inhibition curves through which we could evaluate whether the cells actively died or slowed their proliferation by JQ1 treatment. The results showed that growth inhibition rates were positive even when the cells were treated with 10 μM JQ1, which indicated that the cell cycle was impeded, and active cell death did not occur (Fig. 5A). BrdU and PI staining revealed that proliferating cells (BrdU+ cells) were significantly decreased in both murine and canine HSA cell lines by JQ1 treatment (Fig. 5B). propidium iodide (PI) signals showed that the percentage of dead cells was slightly increased by JQ1 in ISOS-1, but its extent was significantly lower than in canine HSA cell lines (Fig. 5C). We also examined cell senescence by performing SA-β-gal staining in ISOS-1 treated with DMSO or JQ1. The results indicated that JQ1-treated ISOS-1 showed a significantly higher number of positive cells than DMSO-treated cells (Fig. 5D).

These results suggest that autophagy activation and cell cycle downregulation are induced by JQ1 treatment, and that cell senescence but not apoptosis is caused by JQ1 treatment in ISOS-1.

JQ1 suppresses HSA tumour growth in vivo

Finally, to evaluate the treatment effects of SAHA, VPA, and JQ1 *in vivo*, we treated ISOS-1 tumour-bearing Balb/c mice with SAHA, VPA, or JQ1. The results showed that only JQ1 slowed tumour growth and extended the survival rates (Fig. 6A and B). We also treated JuB2 tumour-bearing KSN/Slc mice with JQ1 and showed that JQ1 also suppressed JuB2 tumour growth (Fig. 6C). These treatments did not cause body weight loss in mice (Fig. S3).

These results suggest that JQ1 has suppressive effects on HSA tumour growth i*n vivo*.

Discussion

HSA tumour cells in clinical cases showed various H3 acetylation levels even in the same tumour tissue. Moreover, this heterogeneity differed depending on the histological pattern. This can be explained by the differentiation status of the tumour cells. Global histone acetylation levels have been reported to be increased as cells differentiate (Ashktorab et al., 2009; Golob et al., 2008). Furthermore, HSA tumour cells forming the solid pattern are considered to be undifferentiated (Göritz et al., 2013). Given that the percentage of tumour cells classified as H3 acetylation-negative was high in the solid pattern, they could be more undifferentiated than other tumour cells. Further research is required to clarify whether global histone acetylation levels reflect the differentiation status of HSA tumour cells.

We demonstrated that SAHA and VPA upregulated inflammatory-related genes. Moreover, SAHA-treated JuB4 and VPA-treated Re12 attracted RAW264 cells. Several reports demonstrated that HDACi activated immune responses and enhanced immune cell functions (Cox et al., 2020; Laengle et al., 2020; Sun et al., 2019); thus, SAHA and VPA could also be used as alternative therapeutics for HSA. In our study, however, SAHA and VPA treatment of ISOS-1 in an immunocompetent mouse model did not suppress tumour growth. This implies that the condition we tested was not able to sufficiently induce the immune response to attack tumour cells. Considering this, co-treatment with other drugs such as doxorubicin or immune checkpoint inhibitors would be beneficial for HSA treatment by further stimulating immune responses (Le et al., 2017; Tubbs and Nussenzweig, 2017；Igase et al., 2020; Maekawa et al., 2017). In the present study, we only showed the results from the RAW264 migration assay, and further studies are required to investigate if canine-derived macrophages exhibit the same results and if the migrated macrophages possess anti-tumour functions.

We revealed that JQ1 suppressed tumour growth in HSA cell lines. Several reports demonstrated that JQ1 or other BETi had anti-tumour effects, and clinical trials are ongoing

(Shorstova et al., 2021; Wen et al., 2019). Given that our results could not demonstrate tumour regression upon JQ1 treatment, further research is required to enhance its efficacy and to identify another BETi that can regress HSA tumour growth *in vivo*.

Conclusions

We demonstrated that HDACi and BETi can be used for HSA treatment. Although further research is required, this work provides useful insights for developing new HSA treatments.

Conflict of interest statement

The authors declare that there is no conflict of interest in this study.

Acknowledgements

We would like to extend our sincerest gratitude to Dr. Hiroki Sakai, Gifu University, for providing canine hemangiosarcoma cell lines. We also acknowledge the efforts of Drs. Mitsuyoshi Takiguchi, Shintaro Kobayashi, and Hironobu Yasui, Faculty of Veterinary Medicine, Hokkaido University for giving useful pieces of advice and constructive discussion. We are grateful to all the members of the Laboratory of Comparative Pathology, Faculty of Veterinary Medicine, Hokkaido University for their helpful discussions, encouragement, and support. This research was supported by KAKENHI Grant-in-Aid for Young Scientists (KA, Number 20K15654) provided by Japan Society for the Promotion of Science. We thank H. Nikki March, PhD, from Edanz (https://jp.edanz.com/ac) for editing a draft of this manuscript.

References

Aoshima, K., Fukui, Y., Gulay, K.C.M., Erdemsurakh, O., Morita, A., Kobayashi, A., Kimura, T., 2018. Notch2 signal is required for the maintenance of canine hemangiosarcoma cancer stem cell-like cells. BMC Vet. Res. 14.

Ashktorab, H., Belgrave, K., Hosseinkhah, F., Brim, H., Nouraie, M., Takkikto, M., Hewitt, S., Lee, E.L., Dashwood, R.H., Smoot, D., 2009. Global histone H4 acetylation and HDAC2 expression in colon adenoma and carcinoma. Dig. Dis. Sci. 54, 2109–2117.

Bankhead, P., Loughrey, M.B., Fernández, J.A., Dombrowski, Y., McArt, D.G., Dunne, P.D., McQuaid, S., Gray, R.T., Murray, L.J., Coleman, H.G., et al., 2017. QuPath: Open source software for digital pathology image analysis. Sci. Rep. 7.

Bechter, O., Schöffski, P., 2020. Make your best BET: The emerging role of BET inhibitor treatment in malignant tumors. Pharmacol. Ther.

Bellarosa, D., Bressan, A., Bigioni, M., Parlani, M., Maggi, C.A., Binaschi, M., 2012. SAHA/Vorinostat induces the expression of the CD137 receptor/ligand system and enhances apoptosis mediated by soluble CD137 receptor in a human breast cancer cell line. Int. J. Oncol. 41, 1486–1494.

Benton, C.B., Fiskus, W., Bhalla, K.N., 2017. Targeting Histone Acetylation: Readers and Writers in Leukemia and Cancer. Cancer J. (United States).

Calcagno, D.Q., Wisnieski, F., Da Silva Mota, E.R., Maia De Sousa, S.B., Costa Da Silva, J.M., Leal, M.F., Gigek, C.O., Santos, L.C., Rasmussen, L.T., Assumpção, P.P., et al., 2019. Role of histone acetylation in gastric cancer: Implications of dietetic compounds and clinical perspectives. Epigenomics.

Claerhout, S., Lim, J.Y., Choi, W., Park, Y.Y., Kim, K.H., Kim, S.B., Lee, J.S., Mills, G.B., Cho, J.Y., 2011. Gene expression signature analysis identifies vorinostat as a candidate therapy for gastric cancer. PLoS One 6.

Clayton, A.L., Hazzalin, C.A., Mahadevan, L.C., 2006. Enhanced Histone Acetylation and Transcription: A Dynamic Perspective. Mol. Cell.

Clifford, C.A., Mackin, A.J., Henry, C.J., 2000. Treatment of canine hemangiosarcoma: 2000 and beyond. J. Vet. Intern. Med.

Cox, D.J., Coleman, A.M., Gogan, K.M., Phelan, J.J., Ó Maoldomhnaigh, C., Dunne, P.J., Basdeo, S.A., Keane, J., 2020. Inhibiting Histone Deacetylases in Human Macrophages Promotes Glycolysis, IL-1β, and T Helper Cell Responses to Mycobacterium tuberculosis. Front. Immunol. 11.

Dobin, A., Gingeras, T.R., 2015. Mapping RNA-seq Reads with STAR. Curr. Protoc. Bioinforma. 51, 11.14.1-11.14.19.

Golob, J.L., Paige, S.L., Muskheli, V., Pabon, L., Murry, C.E., 2008. Chromatin remodeling during mouse and human embryonic stem cell differentiation. Dev. Dyn. 237, 1389–1398.

Göritz, M., Müller, K., Krastel, D., Staudacher, G., Schmidt, P., Kühn, M., Nickel, R., Schoon, H.A., 2013. Canine splenic haemangiosarcoma: Influence of metastases, chemotherapy and growth pattern on post-splenectomy survival and expression of angiogenic factors. J.

Comp. Pathol. 149, 30–39.

Gulay, K.C.M., Aoshima, K., Shibata, Y., Yasui, H., Yan, Q., Kobayashi, A., Kimura, T., 2021. KDM2B promotes cell viability by enhancing DNA damage response in canine hemangiosarcoma. J. Genet. Genomics 48, 618–630.

Guo, P., Chen, W., Li, H., Li, M., Li, L., 2018. The Histone Acetylation Modifications of Breast Cancer and their Therapeutic Implications. Pathol. Oncol. Res.

Han, W., Sun, J., Feng, L., Wang, K.F., Li, D., Pan, Q., Chen, Y., Jin, W., Wang, X., Pan, H., et al., 2011. Autophagy inhibition enhances daunorubicin-induced apoptosis in K562 cells. PLoS One 6.

Hou, Y.J., Dong, L.W., Tan, Y.X., Yang, G.Z., Pan, Y.F., Li, Z., Tang, L., Wang, M., Wang, Q., Wang, H.Y., 2011. Inhibition of active autophagy induces apoptosis and increases chemosensitivity in cholangiocarcinoma. Lab. Investig. 91, 1146–1157.

Huang, P., Almeciga-Pinto, I., Jarpe, M., van Duzer, J.H., Mazitschek, R., Yang, M., Jones, S.S., Quayle, S.N., 2017. Selective HDAC inhibition by ACY-241 enhances the activity of paclitaxel in solid tumor models. Oncotarget 8, 2694–2707.

Igase, M., Nemoto, Y., Itamoto, K., Tani, K., Nakaichi, M., Sakurai, M., Sakai, Y., Noguchi, S., Kato, M., Tsukui, T., et al., 2020. A pilot clinical study of the therapeutic antibody against canine PD-1 for advanced spontaneous cancers in dogs. Sci. Rep. 10.

Jones, P.A., Baylin, S.B., 2007. The Epigenomics of Cancer. Cell.

Josling, G.A., Selvarajah, S.A., Petter, M., Duffy, M.F., 2012. The role of bromodomain proteins in regulating gene expression. Genes (Basel).

Jostes, S., Nettersheim, D., Fellermeyer, M., Schneider, S., Hafezi, F., Honecker, F., Schumacher, V., Geyer, M., Kristiansen, G., Schorle, H., 2017. The bromodomain inhibitor JQ1 triggers growth arrest and apoptosis in testicular germ cell tumours in vitro and in vivo. J. Cell. Mol. Med. 21, 1300–1314.

Kabeya, Y., Mizushima, N., Ueno, T., Yamamoto, A., Kirisako, T., Noda, T., Kominami, E., Ohsumi, Y., Yoshimori, T., 2000. LC3, a mammalian homologue of yeast Apg8p, is localized in autophagosome membranes after processing. EMBO J. 19, 5720–5728.

Kaelin, W.G., McKnight, S.L., 2013. Influence of metabolism on epigenetics and disease. Cell.

Kim, J.H., Graef, A.J., Dickerson, E.B., Modiano, J.F., 2015. Pathobiology of hemangiosarcoma in dogs: Research advances and future perspectives. Vet. Sci.

Kim, Y.D., Park, S.M., Ha, H.C., Lee, A.R., Won, H., Cha, H., Cho, S., Cho, J.M., 2020. HDAC Inhibitor, CG-745, enhances the anti-cancer effect of anti-PD-1 immune checkpoint inhibitor by modulation of the immune microenvironment. J. Cancer 11, 4059–4072.

Laengle, J., Kabiljo, J., Hunter, L., Homola, J., Prodinger, S., Egger, G., Bergmann, M., 2020. Histone deacetylase inhibitors valproic acid and vorinostat enhance trastuzumab-mediated antibody-dependent cell-mediated phagocytosis. J. Immunother. Cancer 8.

Le, D.T., Durham, J.N., Smith, K.N., Wang, H., Bartlett, B.R., Aulakh, L.K., Lu, S., Kemberling, H., Wilt, C., Luber, B.S., et al., 2017. Mismatch repair deficiency predicts response of solid tumors to PD-1 blockade. Science (80-.). 357, 409–413.

Lee, Y.J., Won, A.J., Lee, J., Jung, J.H., Yoon, S., Lee, B.M., Kim, H.S., 2012. Molecular mechanism of SAHA on regulation of autophagic cell death in tamoxifen-resistant MCF-7 breast cancer cells. Int. J. Med. Sci. 9, 881–893.

Li, B., Dewey, C.N., 2011. RSEM: Accurate transcript quantification from RNA-Seq data with or without a reference genome. BMC Bioinformatics 12.

Li, F., Yang, C., Zhang, H.B., Ma, J., Jia, J., Tang, X., Zeng, J., Chong, T., Wang, X., He, D., et al., 2019. BET inhibitor JQ1 suppresses cell proliferation via inducing autophagy and activating LKB1/AMPK in bladder cancer cells. Cancer Med. 8, 4792–4805.

Liu, K.Y., Wang, L.T., Hsu, S.H., 2018. Modification of epigenetic histone acetylation in hepatocellular carcinoma. Cancers (Basel).

Maekawa, N., Konnai, S., Takagi, S., Kagawa, Y., Okagawa, T., Nishimori, A., Ikebuchi, R., Izumi, Y., Deguchi, T., Nakajima, C., et al., 2017. A canine chimeric monoclonal antibody targeting PD-L1 and its clinical efficacy in canine oral malignant melanoma or undifferentiated sarcoma. Sci. Rep. 7.

Maharani, A., Aoshima, K., Onishi, S., Gulay, K.C.M., Kobayashi, A., Kimura, T., 2018. Cellular atypia is negatively correlated with immunohistochemical reactivity of CD31 and vWF expression levels in canine hemangiosarcoma. J. Vet. Med. Sci. 80, 213–218.

Masuzawa, M., Fujimura, T., Tsubokawa, M., Nishiyama, S., Katsuoka, K., Terada, E., Kunita, S., Sakurai, Y., Kato, H., 1998. Establishment of a new murine-phenotypic angiosarcoma cell line (ISOS- 1). J. Dermatol. Sci. 16, 91–98.

Mootha, V.K., Lindgren, C.M., Eriksson, K.F., Subramanian, A., Sihag, S., Lehar, J., Puigserver, P., Carlsson, E., Ridderstråle, M., Laurila, E., et al., 2003. PGC-1α-responsive genes involved in oxidative phosphorylation are coordinately downregulated in human diabetes. Nat. Genet. 34, 267–273.

Morita, A., Aoshima, K., Gulay, K.C.M., Onishi, S., Shibata, Y., Yasui, H., Kobayashi, A., Kimura, T., 2019. High drug efflux pump capacity and low DNA damage response induce doxorubicin resistance in canine hemangiosarcoma cell lines. Res. Vet. Sci. 127, 1–10.

Murai, A., Asa, S.A., Kodama, A., Hirata, A., Yanai, T., Sakai, H., 2012. Constitutive phosphorylation of the mTORC2/Akt/4E-BP1 pathway in newly derived canine hemangiosarcoma cell lines. BMC Vet. Res. 8.

Pagiatakis, C., Musolino, E., Gornati, R., Bernardini, G., Papait, R., 2021. Epigenetics of

aging and disease: a brief overview. Aging Clin. Exp. Res.

Pratap, J., Akech, J., Wixted, J.J., Szabo, G., Hussain, S., McGee-Lawrence, M.E., Li, X., Bedard, K., Dhillon, R.J., Van Wijnen, A.J., et al., 2010. The histone deacetylase inhibitor, vorinostat, reduces tumor growth at the metastatic bone site and associated osteolysis, but promotes normal bone loss. Mol. Cancer Ther. 9, 3210–3220.

Proske, J., Walter, L., Bumes, E., Hutterer, M., Vollmann-Zwerenz, A., Eyüpoglu, I.Y., Savaskan, N.E., Seliger, C., Hau, P., Uhl, M., 2016. Adaptive immune response to and survival effect of temozolomide-and valproic acid-induced autophagy in glioblastoma. Anticancer Res. 36, 899–906.

Qiu, H., Jackson, A.L., Kilgore, J.E., Zhong, Y., Chan, L.L.Y., Gehrig, P.A., Zhou, C., Bae-Jump, V.L., 2015. JQ1 suppresses tumor growth through downregulating LDHA in ovarian cancer. Oncotarget 6, 6915–6930.

Robinson, M.D., McCarthy, D.J., Smyth, G.K., 2009. edgeR: A Bioconductor package for differential expression analysis of digital gene expression data. Bioinformatics 26, 139–140.

Shorstova, T., Foulkes, W.D., Witcher, M., 2021. Achieving clinical success with BET inhibitors as anti-cancer agents. Br. J. Cancer.

Subramanian, A., Tamayo, P., Mootha, V.K., Mukherjee, S., Ebert, B.L., Gillette, M.A., Paulovich, A., Pomeroy, S.L., Golub, T.R., Lander, E.S., et al., 2005. Gene set enrichment analysis: A knowledge-based approach for interpreting genome-wide expression profiles. Proc. Natl. Acad. Sci. U. S. A. 102, 15545–15550.

Sun, T., Li, Y., Yang, W., Wu, H., Li, X., Huang, Y., Zhou, Y., Du, Z., 2019. Histone deacetylase inhibition up-regulates MHC class I to facilitate cytotoxic T lymphocyte-mediated tumor cell killing in glioma cells. J. Cancer 10, 5638–5645.

Tubbs, A., Nussenzweig, A., 2017. Endogenous DNA Damage as a Source of Genomic Instability in Cancer. Cell.

Uehara, N., Kanematsu, S., Miki, H., Yoshizawa, K., Tsubura, A., 2012. Requirement of p38 MAPK for a cell-death pathway triggered by vorinostat in MDA-MB-231 human breast cancer cells. Cancer Lett. 315, 112–121.

Vandesompele, J., De Preter, K., Pattyn, F., Poppe, B., Van Roy, N., De Paepe, A., Speleman, F., 2002. Accurate normalization of real-time quantitative RT-PCR data by geometric averaging of multiple internal control genes. Genome Biol. 3.

Virani, Shama, Virani, Shami, Colacino, J.A., Kim, J.H., Rozek, L.S., 2012. Cancer epigenetics: a brief review. ILAR J.

Wen, N., Guo, B., Zheng, H., Xu, L., Liang, H., Wang, Q., Wang, D., Chen, X., Zhang, S., Li, Y., et al., 2019. Bromodomain inhibitor jq1 induces cell cycle arrest and apoptosis of glioma stem cells through the VEGF/PI3K/AKT signaling pathway. Int. J. Oncol. 55, 879–895.

West, A.C., Johnstone, R.W., 2014. New and emerging HDAC inhibitors for cancer treatment. J. Clin. Invest.

Xia, Q., Sung, J., Chowdhury, W., Chen, C.L., Höti, N., Shabbeer, S., Carducci, M., Rodriguez, R., 2006. Chronic administration of valproic acid inhibits prostate cancer cell growth in vitro and in vivo. Cancer Res. 66, 7237–7244.

Xu, R., Li, C., Liu, X., Gao, S., 2021. Insights into epigenetic patterns in mammalian early embryos. Protein Cell.

Xue, K., Gu, J.J., Zhang, Q., Mavis, C., Hernandez-Ilizaliturri, F.J., Czuczman, M.S., Guo, Y., 2016. Vorinostat, a histone deacetylase (HDAC) inhibitor, promotes cell cycle arrest and re-sensitizes rituximab- and chemo-resistant lymphoma cells to chemotherapy agents. J. Cancer Res. Clin. Oncol. 142, 379–387.

Yagi, Y., Fushida, S., Harada, S., Kinoshita, J., Makino, I., Oyama, K., Tajima, H., Fujita, H., Takamura, H., Ninomiya, I., et al., 2010. Effects of valproic acid on the cell cycle and apoptosis through acetylation of histone and tubulin in a scirrhous gastric cancer cell line. J. Exp. Clin. Cancer Res. 29.

Yang, W., Hosford, S.R., Traphagen, N.A., Shee, K., Demidenko, E., Liu, S., Miller, T.W., 2018. Autophagy promotes escape from phosphatidylinositol 3-kinase inhibition in estrogen receptor-positive breast cancer. FASEB J. 32, 1222–1235.

Yoshino, H., Ueda, T., Kawahata, M., Kobayashi, K., Ebihara, Y., Manabe, A., Tanaka, R., Ito, M., Asano, S., Nakahata, T., et al., 2000. Natural killer cell depletion by anti-asialo GM1 antiserum treatment enhances human hematopoietic stem cell engraftment in NOD/Shi-scid mice. Bone Marrow Transplant. 26, 1211–1216.

Zheng, H., Zhao, W., Yan, C., Watson, C.C., Massengill, M., Xie, M., Massengill, C., Noyes, D.R., Martinez, G. V., Afzal, R., et al., 2016. HDAC inhibitors enhance T-cell chemokine expression and augment response to PD-1 immunotherapy in lung adenocarcinoma. Clin. Cancer Res. 22, 4119–4132.

Figure legends

Figure 1. Histone acetylation levels in HSA cells are high *in vitro* and heterogenous *in vivo*.

(A) Western blot analysis of acetylated histone H2B, H3, and H4. (B) Representative images of HE and IHC staining in clinical HSA cases. Scale bars = 50 μm. (C) Box plots for normalized nucleus DAB OD mean values in 10 clinical HSA cases. (D) Representative IHC images of the classifications according to normalised acetylated H3 intensities in each histological pattern. Arrowheads indicate the nuclei of tumour cells. (E) Stacked bar graphs indicating the ratio of each staining level in 10 clinical cases. (F) Stacked bar graphs comparing the ratio of each staining level according to the histological patterns in all cases or within each case. $^{*}P < 0.05$, $^{**}P < 0.01$. Fisher's exact test.

Figure 2. SAHA and JQ1 induce apoptosis in HSA cell lines.

(A) Western blot analysis of acetylated H2B, H3, and H4 in canine HSA cell lines (JuB2, JuB4, Re12) and a murine HSA cell line (ISOS-1) treated with DMSO, SAHA, JQ1, or VPA. (B) Phase contrast images of canine and murine HSA cell lines 48 h after treatment with DMSO, SAHA, VPA, or JQ1. Scale bars = 100 μm. (C) Survival curves (top) and IC_{50} values (bottom) of canine and murine HSA cell lines treated with SAHA or JQ1 for 60 h. All samples were analysed in triplicate. Data are plotted as average percentages ± SD. (D) Western blot analysis of cleaved caspase 3 in canine and murine HSA cells treated with DMSO, SAHA, or JQ1. Uncropped images of JuB4 and Re12 are shown in Figure S2A. (E) Annexin V staining of canine and murine HSA cells treated with DMSO, SAHA, or JQ1. (F) Percentages of apoptotic cells (annexin V-positive) in canine and murine HSA cells treated with DMSO, SAHA, or JQ1. All samples were analysed in triplicate. Data are plotted as average percentages ± SD. $^{*}P < 0.05$, $^{**}P < 0.01$. Tukey's *t* test.

Figure 3. SAHA and VPA activate inflammatory responses in HSA cell lines.

(A) (Left) GSEA results in ISOS-1 treated with SAHA (top) or VPA (bottom). Inflammatory-related gene sets are highlighted in red. The number of genes in each gene set is shown next to each bar. (Right) Representative GSEA plots of enriched gene sets in ISOS-1 treated with SAHA (top) or VPA (bottom). (B) RT-qPCR results of genes related to inflammatory responses in ISOS-1 treated with SAHA or VPA. (C) RT-qPCR results of inflammatory-related genes in JuB4 and Re12 treated with SAHA or VPA. (D) Graphical images of migration assay. (E) Quantitative analysis of migrated RAW264 cells co-cultured with SAHA or VPA-treated Re12. $*P < 0.05$, $**P < 0.01$. Tukey's *t* test.

Figure 4. JQ1 treatment induces autophagy in canine and murine HSA cell lines.

(A) Positively (top) or negatively (bottom) enriched gene sets by GSEA in ISOS-1 treated with JQ1 compared with DMSO-treated cells. The number of genes in each gene set is shown next to each bar. (B) Representative GSEA plots of positively (top) and negatively (bottom) enriched gene sets. (C) RT-qPCR of genes related to autophagy (top) and cell cycle (bottom) in ISOS-1 treated with DMSO or JQ1. (D) Western blot analysis of LC3 protein in canine and murine HSA cell lines treated with DMSO or JQ1.

Fig. 5. JQ1 treatment impedes the cell cycle in canine and murine HSA cell lines.

(A) Growth inhibition curve of ISOS-1 treated with JQ1. All samples were analysed in triplicate. Data are plotted as average percentages ± SD. (B) Density plots (left) and quantitative analysis (right) of BrdU-positive cells in canine and murine HSA cell lines treated with DMSO or JQ1. All samples were analysed in triplicate. (C) Histograms of PI-positive cells (left) and quantitative analysis of dead cells (right) in canine and murine HSA

cell lines treated with DMSO and JQ1. All samples were analysed in triplicate. (D) (Left) Representative images of SA-β-gal staining in ISOS-1 treated with DMSO or JQ1. Arrowheads indicate positive cells. (Right) Quantitative analysis of SA-β-gal-positive cells. Positive cells were counted in 10 fields under 200× magnification with a light microscope. The average numbers were plotted with ± SD. Scale bars = 100 μm. *$P < 0.05$, **$P < 0.01$. Student's *t*-test.

Figure 6. JQ1 suppresses HSA tumour growth *in vivo*.

(A) Kaplan–Meier survival curves of ISOS-1-inoculated Balb/c mice treated with DMSO (n=5), SAHA (n=5), VPA (n=4), or JQ1 (n=5). Days were counted after initiating drug treatment. *P*-values were calculated using the log-rank test. (B) Individual growth curves of ISOS-1 tumours in Balb/c mice treated with DMSO, SAHA, VPA, or JQ1 after treatment initiation. (C) (Left) Individual tumour growth curves of JuB2 tumours in KSN/Slc mice treated with DMSO or JQ1. The day when the treatment began was defined as day 1. ***$P < 0.001$. Two-way ANOVA. (Right) Box plots of relative tumour volumes on the last day in KSN/Slc mice treated with DMSO or JQ1. Relative tumour volumes were calculated by dividing the tumour volume on the last day by that at day 1. *$P < 0.05$, Mann-whitney U test.

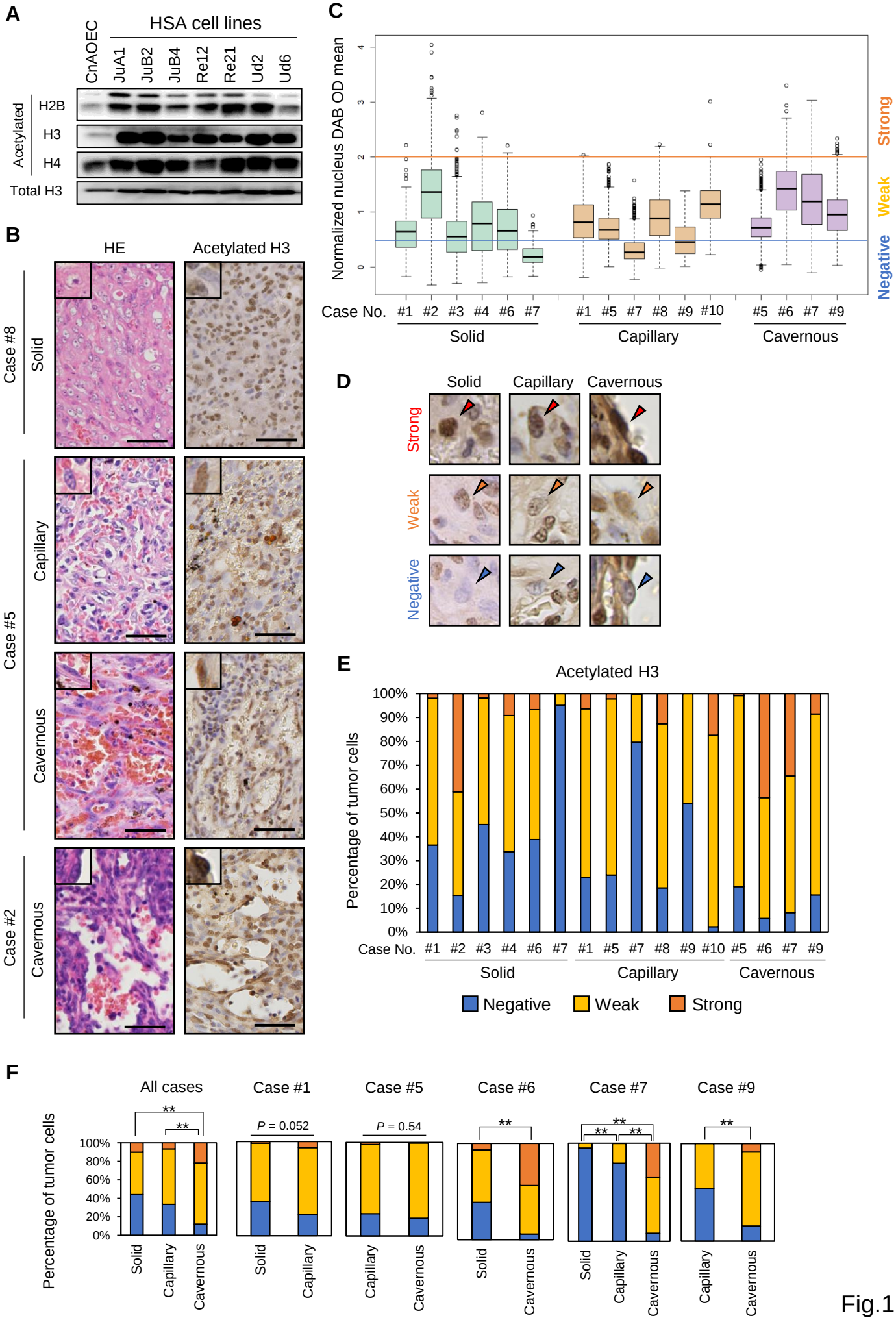
A
HSA cell lines
CnAOEC
JuA1
JuB2
JuB4
Re12
Re21
Ud2
Ud6
Acetylated
H2B
H3
H4
Total H3
B
HE
Acetylated H3
Case #8
Solid
Case #5
Capillary
Cavernous
Case #2
Cavernous
C
Normalized nucleus DAB OD mean
Strong
Weak
Negative
Case No.
#1 #2 #3 #4 #6 #7
#1 #5 #7 #8 #9 #10
#5 #6 #7 #9
Solid
Capillary
Cavernous
D
Solid
Capillary
Cavernous
Strong
Weak
Negative
E
Acetylated H3
Percentage of tumor cells
100%
90%
80%
70%
60%
50%
40%
30%
20%
10%
0%
Case No.
#1 #2 #3 #4 #6 #7
#1 #5 #7 #8 #9 #10
#5 #6 #7 #9
Solid
Capillary
Cavernous
Negative
Weak
Strong
F
All cases
Case #1
Case #5
Case #6
Case #7
Case #9
Percentage of tumor cells
100%
80%
60%
40%
20%
0%
**
P = 0.052
P = 0.54
Solid
Capillary
Cavernous

Fig.1

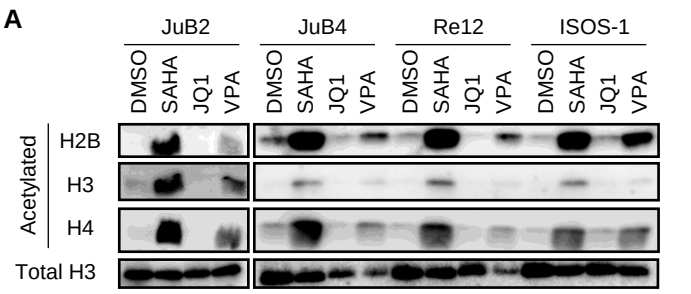

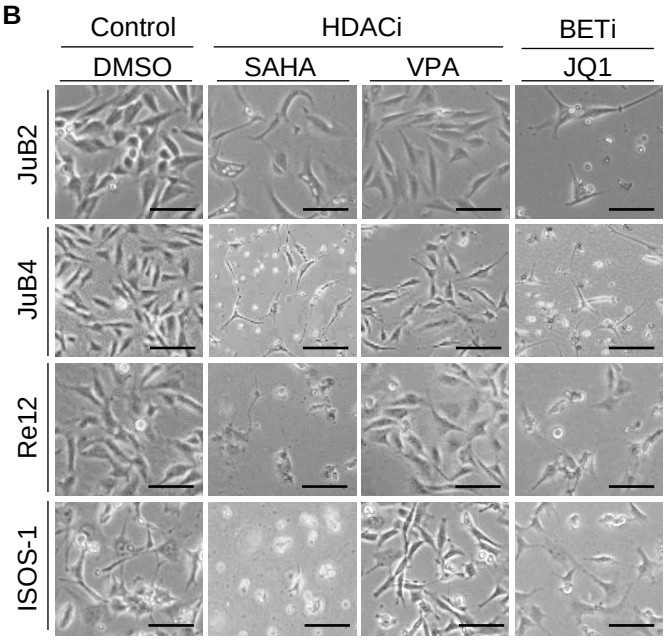

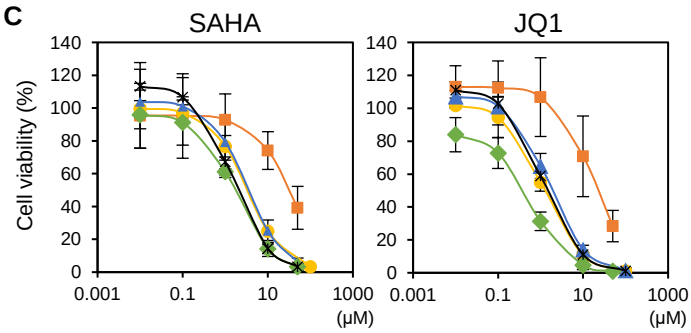

Cell line	SAHA IC_{50} (μM)	JQ1 IC_{50} (μM)
CnAOEC	31.60	21.10
JuB2	3.30	1.22
JuB4	3.47	1.75
Re12	1.61	0.41
ISOS-1	1.84	1.37

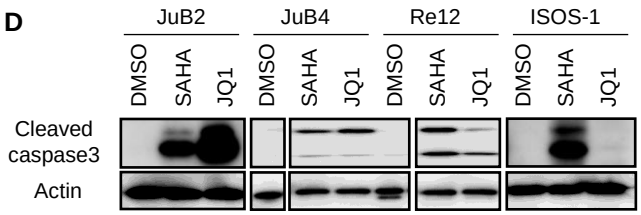

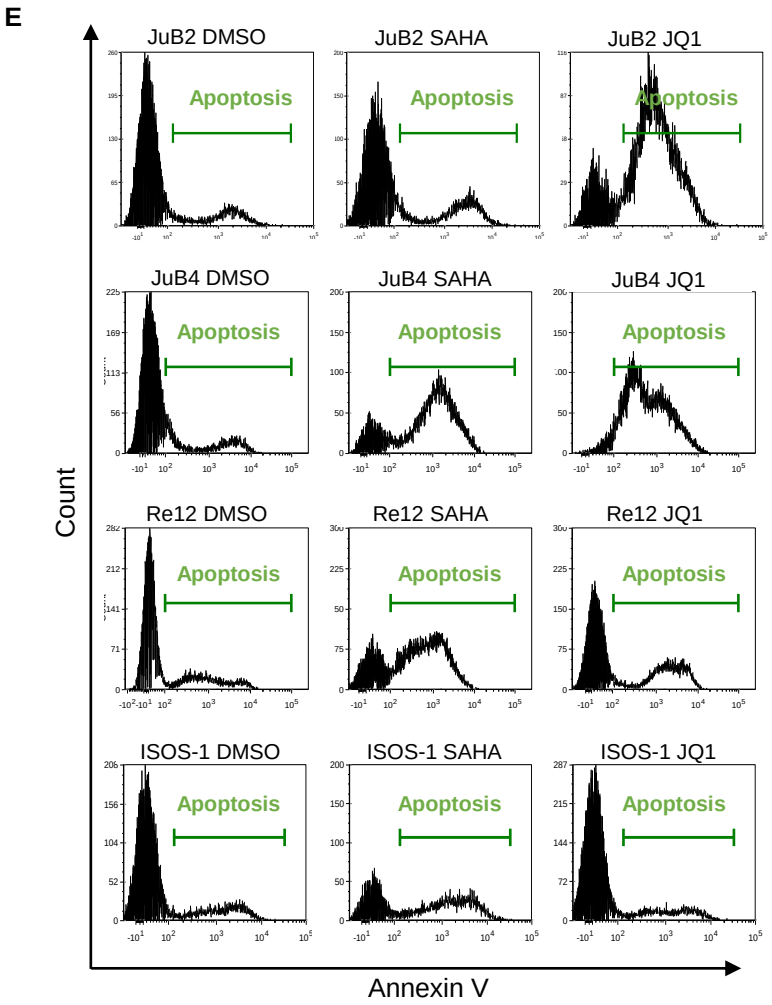

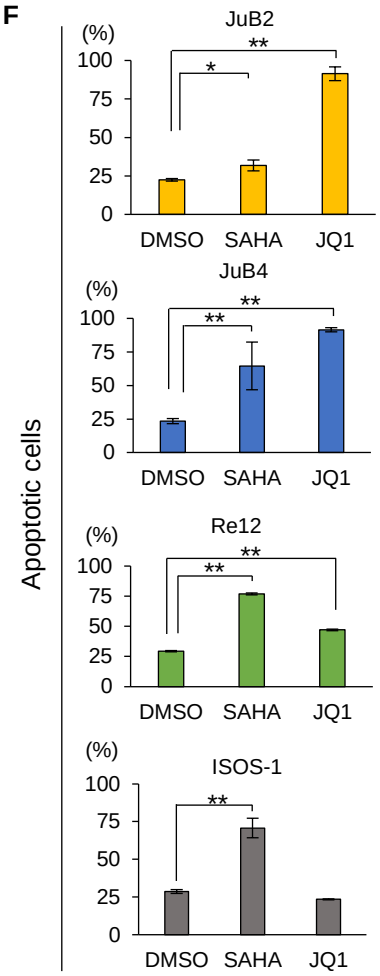

Fig.2

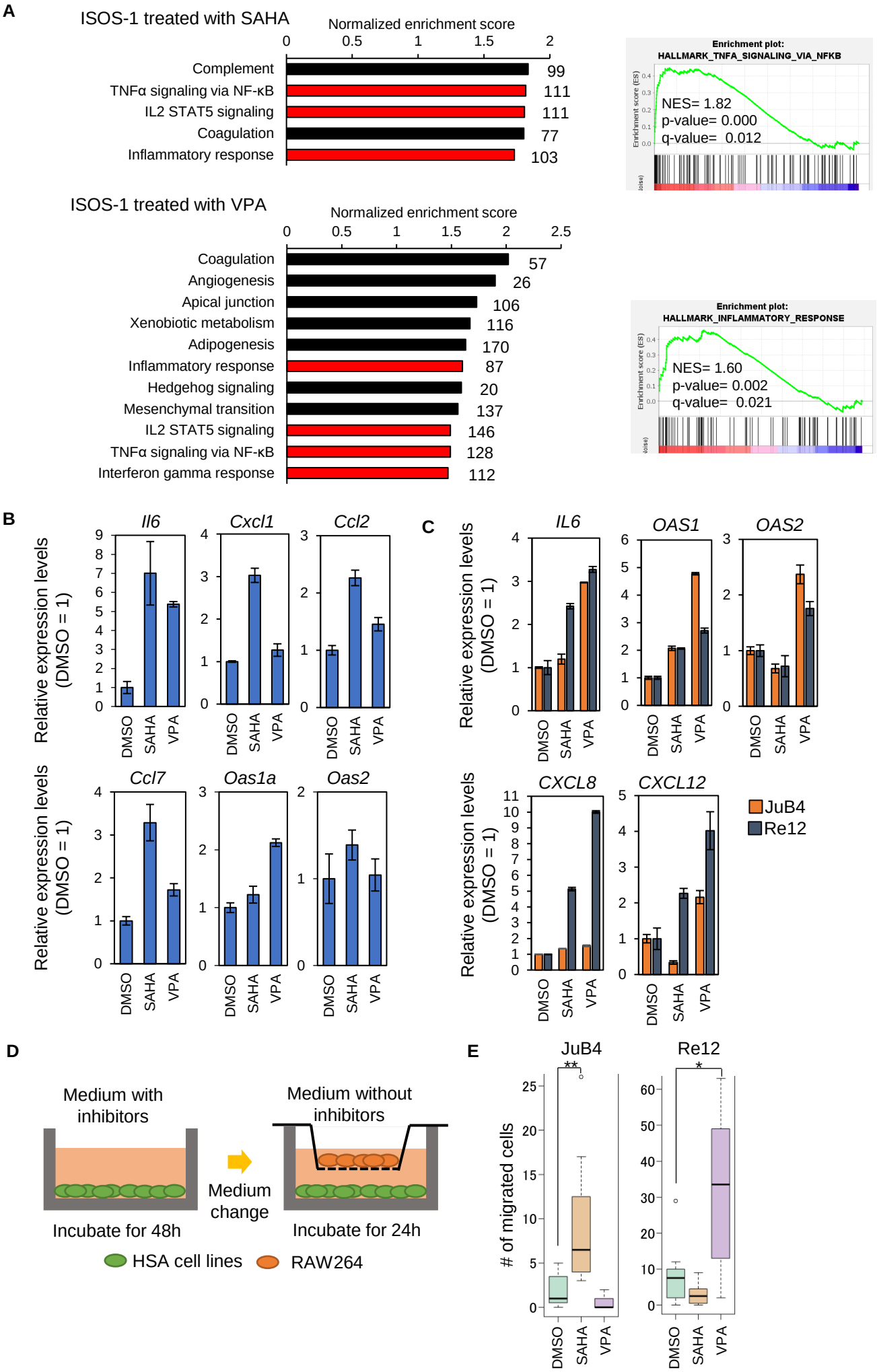
A
ISOS-1 treated with SAHA
Normalized enrichment score
0
0.5
1
1.5
2
Complement
TNFα signaling via NF-κB
IL2 STAT5 signaling
Coagulation
Inflammatory response
99
111
111
77
103
Enrichment plot:
HALLMARK_TNFA_SIGNALING_VIA_NFKB
NES= 1.82
p-value= 0.000
q-value= 0.012
ISOS-1 treated with VPA
Normalized enrichment score
0
0.5
1
1.5
2
2.5
Coagulation
Angiogenesis
Apical junction
Xenobiotic metabolism
Adipogenesis
Inflammatory response
Hedgehog signaling
Mesenchymal transition
IL2 STAT5 signaling
TNFα signaling via NF-κB
Interferon gamma response
57
26
106
116
170
87
20
137
146
128
112
Enrichment plot:
HALLMARK_INFLAMMATORY_RESPONSE
NES= 1.60
p-value= 0.002
q-value= 0.021
B
Il6
Cxcl1
Ccl2
Ccl7
Oas1a
Oas2
Relative expression levels
(DMSO = 1)
DMSO
SAHA
VPA
C
IL6
OAS1
OAS2
CXCL8
CXCL12
JuB4
Re12
D
Medium with
inhibitors
Medium without
inhibitors
Medium
change
Incubate for 48h
Incubate for 24h
HSA cell lines
RAW264
E
JuB4
Re12
# of migrated cells
**
*

Fig.3

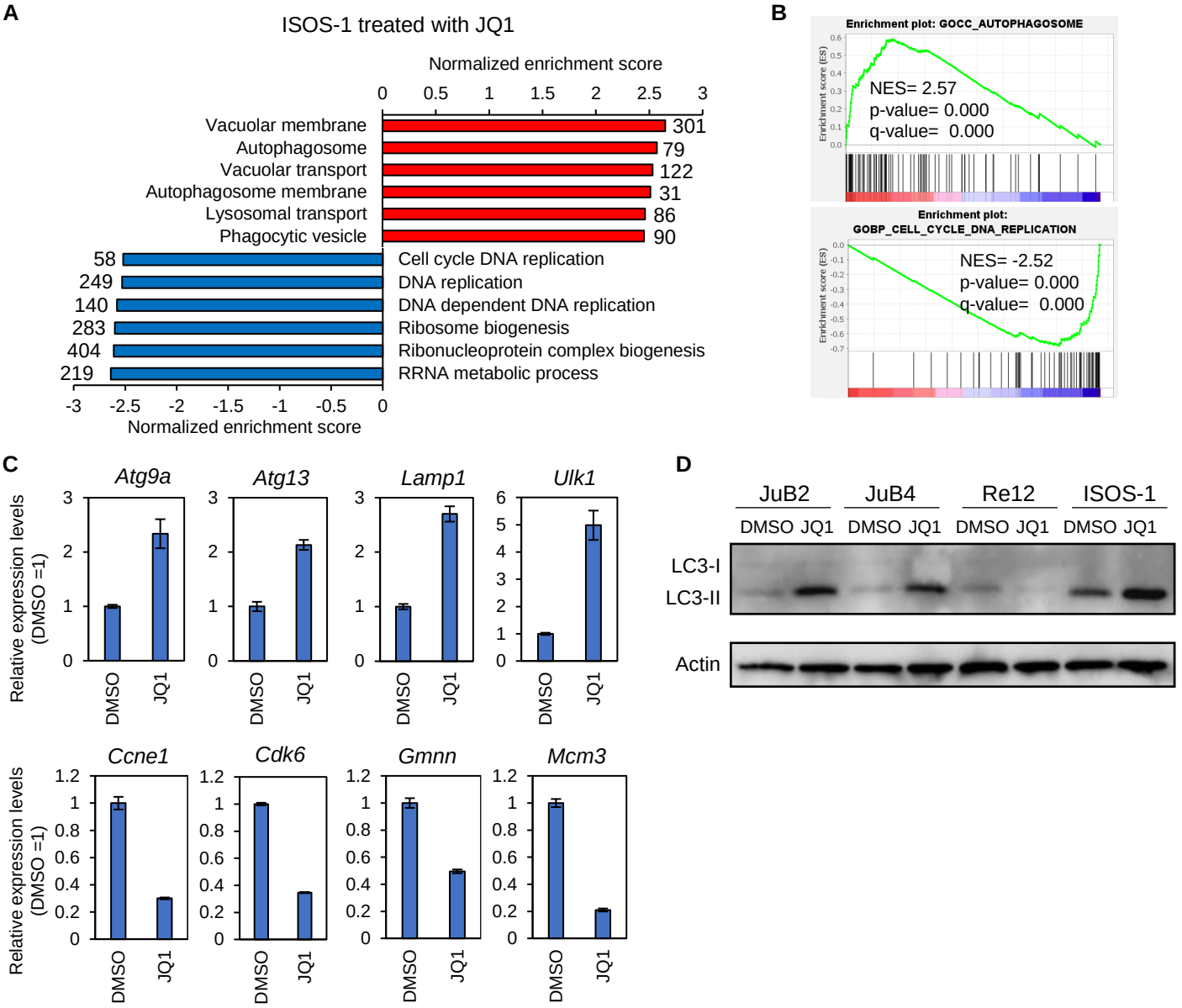
A
ISOS-1 treated with JQ1
Normalized enrichment score
0 0.5 1 1.5 2 2.5 3
Vacuolar membrane 301
Autophagosome 79
Vacuolar transport 122
Autophagosome membrane 31
Lysosomal transport 86
Phagocytic vesicle 90
58 Cell cycle DNA replication
249 DNA replication
140 DNA dependent DNA replication
283 Ribosome biogenesis
404 Ribonucleoprotein complex biogenesis
219 RRNA metabolic process
-3 -2.5 -2 -1.5 -1 -0.5 0
Normalized enrichment score
B
Enrichment plot: GOCC_AUTOPHAGOSOME
NES= 2.57
p-value= 0.000
q-value= 0.000
Enrichment plot:
GOBP_CELL_CYCLE_DNA_REPLICATION
NES= -2.52
p-value= 0.000
q-value= 0.000
C
Atg9a
Atg13
Lamp1
Ulk1
Ccne1
Cdk6
Gmnn
Mcm3
Relative expression levels (DMSO =1)
DMSO
JQ1
D
JuB2
JuB4
Re12
ISOS-1
DMSO JQ1
LC3-I
LC3-II
Actin

Fig.4

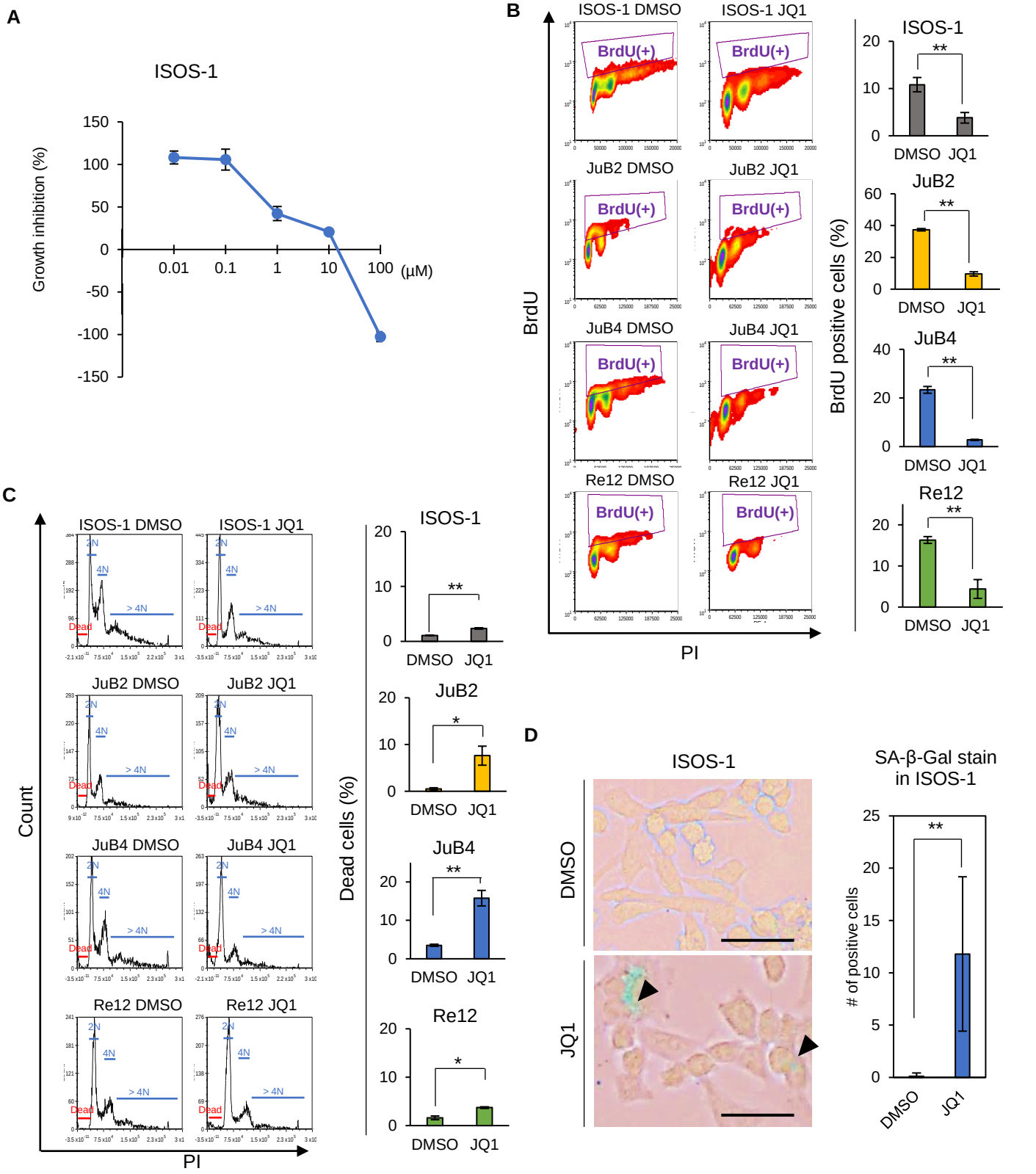
A
ISOS-1
Growth inhibition (%)
150
100
50
0
-50
-100
-150
0.01
0.1
1
10
100
(μM)
B
ISOS-1 DMSO
ISOS-1 JQ1
JuB2 DMSO
JuB2 JQ1
JuB4 DMSO
JuB4 JQ1
Re12 DMSO
Re12 JQ1
BrdU(+)
BrdU
PI
BrdU positive cells (%)
ISOS-1
JuB2
JuB4
Re12
DMSO
JQ1
**
C
Count
PI
2N
4N
> 4N
Dead
Dead cells (%)
*
D
ISOS-1
DMSO
JQ1
SA-β-Gal stain in ISOS-1
# of positive cells

Fig.5

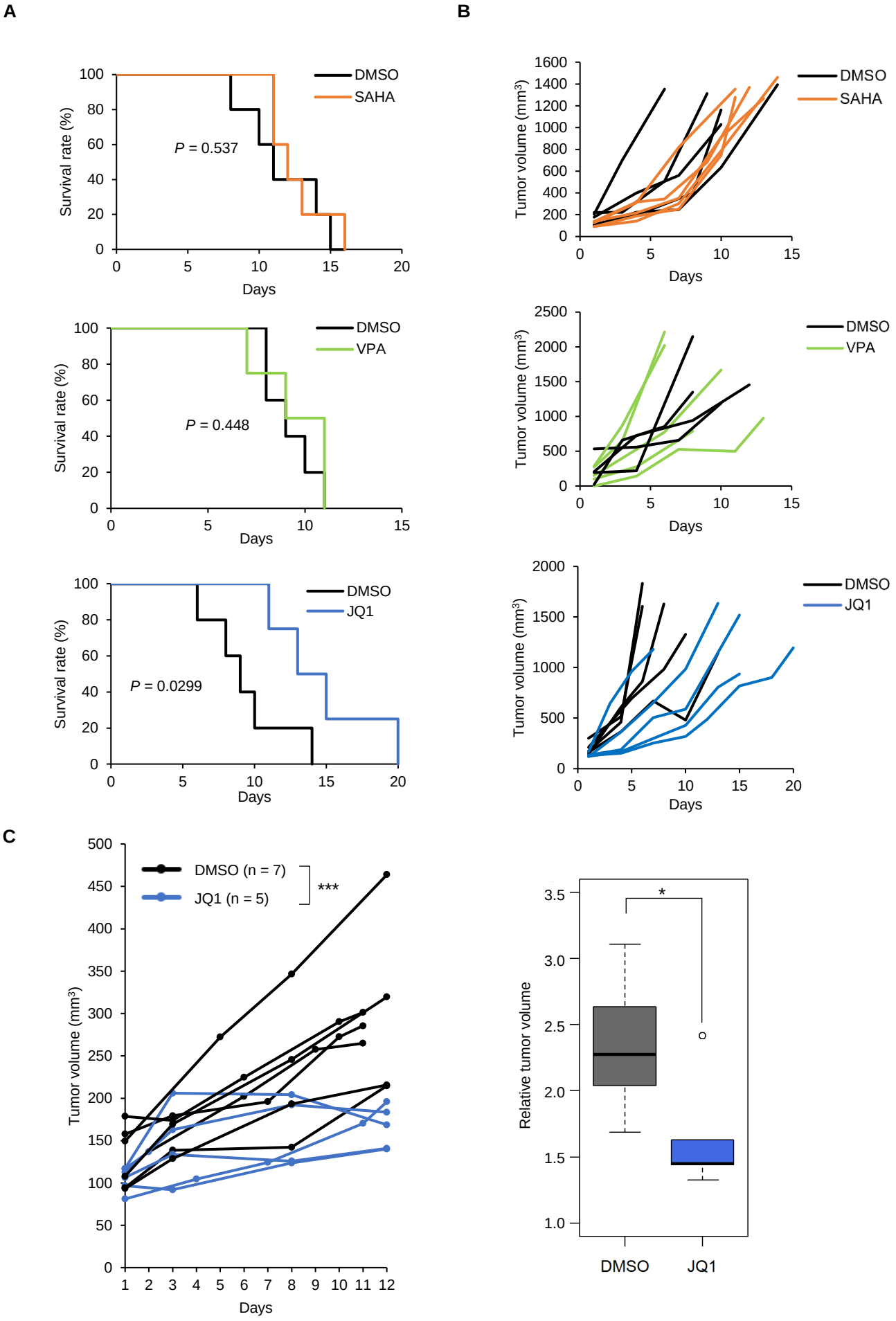
A
B
C
Survival rate (%)
Days
DMSO
SAHA
P = 0.537
VPA
P = 0.448
JQ1
P = 0.0299
Tumor volume (mm³)
DMSO (n = 7)
JQ1 (n = 5)
***
Relative tumor volume
*
DMSO
JQ1

Fig.6